Biophysical Journal

Supporting Material

Productive Cooperation among Processive Motors Depends Inversely on their Mechanochemical Efficiency

Jonathan W. Driver, D. Kenneth Jamison, Karthik Uppulury, Arthur R. Rogers, Anatoly B. Kolomeisky, and Michael R. Diehl

Department of Bioengineering and Department of Chemistry, Rice University, Houston, TX 77030

SUPPLEMENTARY INFORMATION

Modeling Overview

One main goal of the present study is to determine the extent to which our previous optical trapping measurements of two-kinesin detachment forces, velocities and transition rates under load can be reproduced using a model that is parameterized via analyses of single kinesin optical trapping data. Here, single kinesin stiffness, force-velocity, and detachment rate data are used in combination with predictions of load distributions within a multiple motor complex and models of the kinesin detachment and stepping reaction coordinates (all of which are described below) to specify transition rates between different configurations of a two-kinesin complex as it transports a bead against the applied load of the trap (see Figs. 1 and 2 of the main text). The only parameter that is not obtained from single kinesin fits is the zero-load motor binding rate $k_{on[1\rightarrow 2]}(F_{ap}=0)$, which is adopted from a previous experimental / theoretical study (π = 4.7 s^{-1}) (1). No parameters are extracted from fits to our two kinesin data; hence, the plots describing multiple motor behaviors should not be considered as fits to that data. Detailed descriptions of these methods as well as the sensitivities to different model treatments and assumptions are described below.

(1) General modeling considerations

Our 'simulation' method utilizes a set of master equations to compute the time-dependent distribution of microstate populations. Average bead velocities are calculated from the effective stepping rates and the sizes of the bead displacements that they produce. Thus, the calculations are equivalent to data analyses where stalling events are included as zero velocities. Note, this model does not produce individual trajectories, and hence, some analyses in our prior report (2) cannot be applied to the present modeling data (*e.g., the acceleration threshold used to determine transition rates between different load-sharing classes of two-kinesin microstates cannot be calculated computationally using the present approach*).

For all calculations, motor trajectories are constrained to a single microtubule protofilament, and volume exclusion effects that would otherwise prevent motors from binding the same microtubule lattice site are neglected. These choices were made because they simplify computations significantly while still approximating the transport dynamics of the two-kinesin complexes. In general, multiple motor predictions did not change appreciably when we tested a 3-dimensional form of our model with volume exclusions (*incorporating three different parallel protofilaments*) where the motors could occupy explicitly enumerated sites on neighboring protofilaments that produce side-by-side motor-bound geometries. We believe these assumptions are appropriate since most bound geometries of the two-motor complexes are nearly two-dimensional (*planar*) when solved in three dimensions. Furthermore, the presence of parallel protofilaments should allow motors to occupy the same longitudinal (*along the axis of the microtubule*) position, giving the appearance of violating volume exclusion in two dimensions.

For calculations of multiple motor behaviors in a static optical trap (*where motors experience time-dependent loads*), it is assumed that cargo transport begins with the binding of a single motor to a microtubule lattice site where the applied load on the bead is zero. As the bead moves forward, the number of filament-bound motors and the spacing between their microtubule binding sites changes in time depending on how motors step along, bind to, or

detach from the filament. Unbound motors are able to bind sites on the microtubule that are either in front of or behind motors that are already filament-bound. Partial detachment of a complex via the unbinding of one motor and the associated retraction of the bead back towards the trap center position is allowed; the unbound motor can rebind the filament after such events. Complete bead / assembly detachment (*i.e., when a singly-bound motor releases from the filament*) ends a 'run'; rebinding after such events is not allowed.

The above constraints were also implemented for analyses of the stationary-state dynamics of two-kinesin complexes under constant applied loads with minimal alterations. This treatment emulates the experimental conditions that can be generated in an optical force clamp at long timescales. Here, microstate distributions were found by evolving the system for 2 seconds. We find that the two-motor system converges to the steady-state distribution within this timeframe given any initial distribution of two-motor bound configurations that we tested. Of note, 2 seconds substantially exceeds the relaxation time constant at any given force (<0.5 sec, see Fig. 6A).

(2) Mechanical calculations

In order to calculate motor stepping, binding and detachment rates, the vectorial forces that the motors experience must be approximated reliably. These forces are a function of the points of attachment of the motors to both the bead and the microtubule, as well as the position of the bead within the optical trap. When the forces are not balanced, the bead adjusts its position rapidly as seen in the experimental data, where the bead moves almost instantaneously in response to the steps and detachment of the motors. It is therefore reasonable to assume that the forces within the system are balanced between transitions, and that calculating the forces on the motors requires finding these force-balanced geometries. We refer to these force-balanced geometries as "microstates".

2.1 Finding force-balanced microstate geometries

To find force-balanced microstate geometries, a mechanical model of the trap-bead-motor system was created. Given positions of the motors on the bead and on the microtubule, as well as the position of the trap and the position and orientation of the bead, the model is able to calculate the forces within the system. Calculations of force-balanced geometries begin with an estimate of the bead's position and orientation and initial calculations of force distributions within the system. If imbalanced, the direction and magnitude of the net imbalance is used to estimate a new bead position. Imbalances can occur both in the 'x' direction (*along the microtubule axis*) and in the torque on the bead (*the motors always pull the bead down to the microtubule surface - the trap is weak in this direction - so it is initially placed there and no imbalances in the 'z' direction occur*). The process of assessing force balance and repositioning of the bead is repeated reiteratively until the net imbalance decreases below a threshold of 0.1 fN in all directions, at which point it is deemed negligible. The resulting system geometry is taken as the force-balanced microstate geometry.

Once the force-balanced microstate geometry is found, the mechanical energy of that geometry is calculated. This energy, which we call "configurational energy", is equal to the sum of the stretching energies of the trap (a linear spring) and the motors (nonlinear springs, see Section 2.3). As stated in the text, configurational energies can be expressed by:

$$E_{\mathrm{config}} = \tfrac{1}{2}\kappa_{\mathrm{T}}(x_{\mathrm{T}} - x_b)^2 + \textstyle\sum_{\mathrm{M}} \int_{l_{\mathrm{o}}}^{l_{\mathrm{ax}}} \left\| \vec{F}_{\mathrm{ax}} \right\| dl \qquad \textbf{(S1)}$$

Here, κ_{T} is the stiffness of the trap, x_{T} is the position of the trap, x_{b} is the position of the bead, l_{ax} is the head-to-tail length of the kinesin motor, l_{o} is its unstretched length, and F_{ax} is the restoring force along the axis of the motor. The summation is carried out over all microtubule-attached motors (M).

2.2 Stiffness of a single kinesin motor

As in other published reports (3), we observed a nonlinear, strain-induced stiffening of our single kinesin motors in the optical trap as shown in Fig. 2A of the main text. These stiffness data were calculated from thermally-driven fluctuations of beads along the axis of the microtubule, and thus represent a projection of the motor's head-to-tail stiffness, $\kappa_{\mathrm{M}}(l_{ax})$, along this axis (*the projection is denoted* $\kappa_{\mathrm{M,x}}$). The motor's head-to-tail stiffness is a function of its stretched length l_{ax}, which changes with the force applied to the bead:

$$\kappa(l_{\mathrm{ax}}) = \frac{a}{1-b*\exp(c*(l_{\mathrm{ax}}-l_{\mathrm{o}}))} + d \qquad \textbf{(S2)}$$

This empirical function was chosen to approximate the composite elasticity of the motor since the motors are linked to the beads via multiple mechanical elements (*i.e., the engineered polymers, and the streptavidin-biotin bead coating*), and a mechanistic (*analytical)* functional form of motor elasticity is therefore exceedingly difficult to define. Given $\kappa_{\mathrm{M}}(l_{ax})$, $\kappa_{\mathrm{M,x}}(F_{ap})$ is found by using the mechanical model to test the resistance of the bead to changes in its position across a range of applied loads. A standard MALAB fitting routine (nlinfit) was used to fit equation S2 to our stiffness data (taking a, b, c, and d as fitting parameters); $\kappa_{\mathrm{M,x}}(F_{ap})$ was recalculated each time a new set of parameter values was tested by the routine.

(3) <u>Transitions between microstates</u>

3.1 The need to consider load-rate-dependent effects on motor detachment

We implemented a model of motor-microtubule detachment that allows one to account for load-rate-dependent effects instead of a simple Kramer's theory for several reasons. First, Kramer's-like exponential fits under-approximate the detachment rates measured in our single kinesin experiments at low forces (Fig. 2C of the text and Fig. S1A). Secondly, two-kinesin detachment force histograms contain a second peak at 9.5 pN that is not present on our experimental data if this function is used to parameterize the rates of motor detachment under load (*i.e., it yields a higher motor-microtubule affinity and a much lower* $k_{off[2\rightarrow 1]}$ *than is found in our two-kinesin assays*). This result is described in more detail in section 5 below.

The affinity of many non-covalent bonds is known to depend not only on the force applied to them at any given time, but also on the rate at which that force was accumulated (4). The disagreement described above therefore indicates such effects could be altering the dynamics of our two-kinesin complexes in the optical trap. In general, loading rates should influence bead detachment in both single kinesin and multiple kinesin assays. However, in the latter case, detachment and loading rates for each motor in the two-motor experiments can differ for each motor in the complex when the loads are not shared equally. As stated in the main text, loading rates will depend on how load distributions within a complex change in time; in most cases, this behavior appears to reduce the load rate experienced by a motor, and hence, motor detachment rates will correspond more closely to their steady-state (load-rate-independent) behaviors. Thus, parameterizing motor detachment kinetics from single kinesin detachment data requires extraction of load-rate-independent trends. Below, we describe how

single kinesin data is used to approximate a simple two-state reaction coordinate describing motor-microtubule detachment, and how this coordinate is used to calculate load-rate-dependent and load-rate-independent detachment behaviors when modeling multiple motor dynamics.

3.1.1 Load-rate-dependent model of motor detachment. The dependence of detachment rate on loading rate can be explained by a multi-state attachment/detachment model (24), which stipulates that the two species (the motor and the microtubule in this case) stably bind in two or more states with different affinities. For the treatment employed here, motor detachment is assumed to occur along a two-state reaction coordinate (Fig. S1) that contains one state representing a "tightly-bound" state of the motors (T) and a second state corresponding to a "loosely-bound" state (L). There are also two energy barriers and transition states (TS_1 and TS_2) in between these states and the unbound state of the motors. Of note, if the motors are in the tightly-bound state, they must transition through the loosely-bound state to reach the unbound state. This has an important implication: *the observed detachment rate at any given time is proportional to the probability that the motor is in the loosely-bound state*.

$$k^{\mathrm{off}} = \frac{B_L}{B_L + B_T}\, k_{B_L \to U} \qquad \textbf{(S3)}$$

Transition rates between states within the reaction coordinate in Fig. S1 depend on the activation energy for the transition (*i.e., the free energy difference between* T *and* TS_2 *or* L *and* TS_1), and can be calculated using an Arrhenius relation:

$$k = A\, e^{-E_a / k_{\mathrm{B}} T} \qquad \textbf{(S4)}$$

We assume that the pre-exponential factor A, known as the "attempt frequency", has a value of $2.08 * 10^{10}$ for all transitions (P.L. Houston, *Chemical Kinetics and Reaction Dynamics*, McGraw Hill, New York, 2001). It should be noted that the exact value of this pre-exponential factor does not affect the results of our model significantly.

The following rate equations describe the evolution of the bound state populations of a motor in the two-state model:

$$\frac{d}{dt} B_T = -k_{B_T \to B_L}\, B_T + k_{B_L \to B_T}\, B_L \qquad \textbf{(S5)}$$

$$\frac{d}{dt} B_L = k_{B_T \to B_L}\, B_T - \left(k_{B_L \to B_T} + k_{B_L \to U}\right) B_L \qquad \textbf{(S6)}$$

In these equations, B_L and B_T are the loosely- and tightly-bound state populations, respectively. A change in load influences the rate constants by tilting the energy landscape. Thus, in order to transition between states along the reaction coordinate, work must be performed against that load. The energies for all of the different states Φ at positions x_Φ along the coordinate are therefore given by:

$$E_\phi = E_{\phi, F_{ap}=0} - F_{ap}\, x_\phi \qquad \textbf{(S7)}$$

3.1.2 Model fit to single-kinesin detachment rate data. To fit the single-kinesin detachment rate data presented in Fig. 2C, the loosely-bound fraction of motors (*which, again, corresponds to observed detachment rate through equation S3*) as a function of the static optical trap's load is determined from the time-dependent solution to equations S5 and S6. Here, the load is assumed to change in time in accordance with the single kinesin *F-V* relationship that is produced in the static optical trap where bead velocities are attenuated by the stretching of motor-bead linkages as the load builds on the motor (*i.e., these curves are used without the typical adjustments to bead velocities that are made to correct for the influence of motor*

compliance). The initial populations of B_L and B_T are assumed to correspond to a steady-state distribution of bound states that would be produced in the absence of and applied load (*this calculation is discussed in the next subsection*). The results of the time-dependent calculation change as the positions and zero-load energies of the states in the reaction coordinate are changed. A MATLAB fitting algorithm (nlinfit) was used to adjust these positions and energies to minimize the error between the calculated detachment rates and the data.

3.1.3 Calculating load-rate-independent motor-microtubule detachment rates. Motor detachment rates should be invariant in time when applied loads are held constant. Thus, in this case, detachment rates are determined by first solving for the fraction $B_L/(B_T+B_L)$ using a steady-state approximation:

$$\frac{d}{dt}\left[\frac{B_L}{B_T+B_L}\right] = 0 = \frac{(B_T+B_L)*\frac{d}{dt}B_L - B_L*\left(\frac{d}{dt}B_T+\frac{d}{dt}B_L\right)}{(B_T+B_L)^2}$$

$$= B_T * \frac{d}{dt}B_L - B_L * \frac{d}{dt}B_T \qquad \textbf{(S8)}$$

Using equations S5 and S6 to define the terms $\frac{d}{dt}B_L$ and $\frac{d}{dt}B_T$, we arrive at a quadratic equation relating B_L to B_T that can be solved for B_T.

$$B_T = \frac{k_{(B_L\to B_T)} - k_{(B_T\to B_L)} + k_{(B_L\to U)} + \sqrt{k_{(B_L\to B_T)}{}^2 + [k_{(B_T\to B_L)} - k_{(B_L\to U)}]^2 + 2\cdot k_{(B_L\to B_T)}\,[k_{(B_T\to B_L)} + k_{(B_L\to U)}]}}{2\,k_{(B_T\to B_L)}} B_L$$

Rearrangement allows the fraction of loosely-bound motor at constant load in equation S3 to be calculated.

$$\frac{B_L}{B_L+B_T} = \frac{1}{1+\frac{k_{(B_L\to B_T)} - k_{(B_T\to B_L)} + k_{(B_L\to U)} + \sqrt{k_{(B_L\to B_T)}{}^2 + [k_{(B_T\to B_L)} - k_{(B_L\to U)}]^2 + 2\cdot k_{(B_L\to B_T)}\,[k_{(B_T\to B_L)} + k_{(B_L\to U)}]}}{2\,k_{(B_T\to B_L)}}} \qquad \textbf{(S9)}$$

This relationship is implicitly a function of applied load because the rate constants (k) are functions of the applied load through equations S4 and S7.

3.2 Calculating motor-microtubule binding and stepping rates

Motor-microtubule binding rates k^{on} were calculated using detachment rates and the detailed balance equation.

$$\frac{k^{\mathrm{on}}}{k^{\mathrm{off}}} = \frac{k_{\mathrm{o}}^{\mathrm{on}}}{k_{\mathrm{o}}^{\mathrm{off}}} * \exp\left(-\frac{\Delta E_{\mathrm{config}}}{k_{\mathrm{B}}\mathrm{T}}\right) \qquad \textbf{(S10)}$$

Here, k^{off} is the detachment rate when the load is held constant on the motor. The subscript "o" indicates the zero-strain value of the binding or detachment rate. The change in configurational energy is calculated between the single-motor-bound microstate and the two-motor-bound microstate of the transition.

Motor stepping rates were calculated using the model of Fisher and Kim described in the main text.

(4) Numerical calculation methods

4.1 Defining and solving master equations

We use the rates of transition between microstates described in Section 3 to define a system of ordinary differential equations, the "master equations", describing the evolution of the motor system probabilistically as it transitions through all enumerated microstates of the model. The generalized set of master equations for a two-motor system can be written as follows:

$$\frac{d\psi^0}{dt} = \sum_i k_i^{\text{off}}\,\psi_i^a + \sum_j k_j^{\text{off}}\,\psi_j^b \tag{S11}$$

$$\frac{d\psi_i^a}{dt} = u_{(i-1)\to i}\,\psi_{(i-1)}^a + w_{(i+1)\to i}\,\psi_{(i+1)}^a - \left(k_i^{\text{off}} + \sum_j k_{i\to(i,j)}^{\text{on}} + u_{i\to(i+1)} + w_{i\to(i-1)}\right)\psi_i^a + \sum_j k_{(i,j)\to i}^{\text{off}}\,\psi_{(i,j)}^{a,b} \tag{S12}$$

$$\frac{d\psi_j^b}{dt} = u_{(j-1)\to j}\,\psi_{(j-1)}^b + w_{(j+1)\to j}\,\psi_{(j+1)}^b - \left(k_j^{\text{off}} + \sum_i k_{j\to(i,j)}^{\text{on}} + u_{j\to(j+1)} + w_{j\to(j-1)}\right)\psi_i^b + \sum_i k_{(i,j)\to j}^{\text{off}}\,\psi_{(i,j)}^{a,b} \tag{S13}$$

$$\begin{aligned}\frac{d\psi_{(i,j)}^{a,b}}{dt} = {} & \left(k_{i\to(i,j)}^{\text{on}}\,\psi_i^a + k_{j\to(i,j)}^{\text{on}}\,\psi_j^b\right) + u_{(i-1,j)\to(i,j)}\psi_{(i-1,j)}^{a,b} + u_{(i,j-1)\to(i,j)}\,\psi_{(i,j-1)}^{a,b} + w_{(i+1,j)\to(i,j)}\,\psi_{(i+1,j)}^{a,b} + \\ & w_{(i,j+1)\to(i,j)}\,\psi_{(i,j+1)}^{a,b} - \left[k_{(i,j)\to i}^{\text{off}} + k_{(i,j)\to j}^{\text{off}} + u_{(i,j)\to(i+1,j)} + u_{(i,j)\to(i,j+1)} + w_{(i,j)\to(i-1,j)} + w_{(i,j)\to(i,j-1)}\right]\psi_{(i,j)}^{a,b}\end{aligned} \tag{S14}$$

In these equations, ψ denotes the probability of an individual microstate. Its superscript indicates whether the cargo is completely detached (ψ^0), bound via only one motor (ψ^a or ψ^b), or via both motors in the complex ($\psi^{a,b}$). The subscripts i and j denote the microtubule lattice-site position of the motors. Microstate transition rates for motor binding (k^{on}), detachment (k^{off}), and stepping (u and w) also use i and j indices to indicate the initial and final microstates of the system for that transition (see Section 3).

Note, a different notation was used to specify individual microstate transitions in the master equations to distinguish them from average rates describing how rapidly motors transition between different classes of microstates (*e.g.,* $k_{off[2\to1]}(F_{ap})$ *in the text describes the average of all transitions where a single motor in a complex detached at a specified load,* F_{ap}). In addition, equations S11-S14 clearly separate detachment transitions from motor stepping transitions, meaning these reaction coordinates are uncoupled in our model. This approximation is appropriate for kinesins since fitted pre-factors in equations 2 and 3 in the text, as well as those of Fisher and Kim, both dictate that kinesin will primarily occupy the intermediate state position along its stepping reaction coordinate; steps are fast and the occupancy of other sub-step positions is small. Furthermore, the ground state and the intermediate state positions are very close to one another, so the difference between their strain energies and detachment rates is negligible.

To evaluate dynamic properties of motor protein complexes, we utilize the following method. The master equations can be written formally in matrix form, with Ψ being a vector containing all microstate populations and A being the transition rate matrix,

$$\frac{\mathrm{d}}{\mathrm{dt}}\Psi = \mathrm{A}\,\Psi \tag{S15}$$

From this matrix equation and the definition of the time derivative, a forward Euler approximation can be obtained for evolving a distribution of microstates in small time steps (from t to time $t+\Delta t$):

$$\Psi_{t+\Delta t} \approx \Psi_t + \Delta t\,\mathrm{A}\,\Psi_t \tag{S16}$$

This approximation can be used reiteratively to obtain numerical estimates of time-dependent distributions of microstate populations (Fig. 4).

4.2 Calculating average microstate probabilities, bead velocities, and detachment forces

4.2.1 Using microstate probabilities to calculate average (observed) behaviors. To calculate experimental observables, time-dependent distributions of microstate populations are first integrated over time to give a weighting that describes the relative probabilities of microstates over the entire course of the numerical calculation. These probabilities can be used to calculate measured properties such as the bead velocity and kinetic rates via (Fig. 3):

$$\langle O \rangle = \frac{\sum_{i,j} O_{i,j} \int_0^{t_{\mathrm{end}}} \psi_{(i,j)}(\mathrm{t})\,\mathrm{dt}}{\sum_{i,j} \int_0^{t_{\mathrm{end}}} \psi_{(i,j)}(\mathrm{t})\,\mathrm{dt}} \qquad (\mathbf{S17})$$

The letter O denotes a generalized observable, $<O>$ is its expectation (*average*) value, and $O_{i,j}$ is the value of the observable for the microstate (i,j). The state sum can be extended over all microstates (*single- and two-motor-bound*) or over a specific subset (e.g., two-motor-bound only), depending on what is being measured.

4.2.2 Bead velocity. Bead velocity is a function of the stepping rates of the motors driving its motion and the displacement that those stepping events produce in the bead's center position.

$$V_{i,j} = u_{(i,j)\to(i+1,j)}\,\Delta x^{\mathrm{B,eq}}_{(i,j)\to(i+1,j)} + u_{(i,j)\to(i,j+1)}\,\Delta x^{\mathrm{B,eq}}_{(i,j)\to(i,j+1)} + w_{(i,j)\to(i-1,j)}\,\Delta x^{\mathrm{B,eq}}_{(i,j)\to(i-1,j)} + w_{(i,j)\to(i,j-1)}\Delta x^{\mathrm{B,eq}}_{(i,j)\to(i,j-1)} \qquad (\mathbf{S18})$$

The quantity $\Delta x^{\mathrm{B,eq}}_{\mathrm{trans}}$ refers to the change in the bead's steady-state position across the transition in the subscript. This method is valid for both variable and constant load numerical calculations. Average bead velocities are calculated using the $V_{i,j}$ in equation S18 as the observable (*O*) in equation S17.

4.2.3 Detachment force distribution. Our theoretical approach allows us to describe detachment processes in a two-motor system. A detachment force histogram (Fig. 3A *bottom, grey bars*) presents all individual motor detachment events predicted to occur over the course of a numerical calculation. In a two-motor system, this includes the detachment of either the leading (*gold bars*) or the trailing (*blue bars*) motor in two-motor-bound microstates, as well as detachment from single-motor-bound microstates (*red bars*). In the transition rate model, these "events" reflect changes in microstate densities that arise from transitions out of two-motor-bound microstates to a single-motor-bound microstate, or from a single-motor-bound microstate to the unbound microstate. An example of this calculation can be described as follows: for a generic two-motor-bound detachment transition, the total population $\psi^{\mathrm{tot}}_{(i,j)\to i}$ that passes from the two-motor-bound microstate $\psi^{a,b}_{(i,j)}$ into the single-motor-bound microstate ψ^{a}_{i} during the simulation is:

$$\psi^{\mathrm{tot}}_{(i,j)\to i} = \sum_{\mathrm{t}=0}^{\mathrm{t_{end}}} \Delta\mathrm{t}\; k^{\mathrm{off}}_{(i,j)\to i}\; \psi^{a,b}_{(i,j)}(\mathrm{t}) \qquad (\mathbf{S19})$$

Here, the detachment force is taken as the force on the cargo (F_{ap}) when the system was in the two-motor-bound microstate. All other single- and two-motor detachment transitions are treated analogously. The heights of the bars of the detachment force histogram are equal to the sum of every ψ^{tot} whose detachment force falls within the bounds of the bin, normalized to the height of the tallest bar in the histogram.

4.3 Evaluating multiple-motor relaxation times

At any given applied load, the observed behavior of the two-kinesin system will depend on the distribution of microstates that it occupies. However, that distribution will also evolve in time towards a steady-state distribution at “long” times if the applied load is held constant. If loads on the cargo change more quickly than this convergence timescale, then the behavior of the system will be a function of both the applied load and the loading rate, analogous to the case of the single-motor detachment rates discussed in Section 3.1. We refer to these convergence timescales as "relaxation" times (reported in Fig. 5), which are defined as the exponential rate of convergence of the cargo velocity to its long-time value in the constant load experiment when the initial microstate populations are set to their steady-state values for a loading force 1 pN below that of the current experiment. For example, to calculate τ_{relax} for a two-motor system under a 5 pN load, one would initialize the microstate distribution to that of the long-time limit distribution under a 4 pN load, then simulate the evolution of the distribution, keeping track of the average velocity at each time point. The dependence of the average velocity on time is then fit to the exponential function:

$$V_{\mathrm{av}}(t) = A - B\, e^{-t/\tau_{\mathrm{relax}}} \qquad \textbf{(S20)}$$

The values of τ_{relax} are given in Fig. 5A (*left*), as well as the same values normalized by the "stepping" timescale τ_{step} (*right*), which is the average time it takes for the bead to travel 8.2 nm under the same constant load at steady-state (*i.e. this time is simply 8.2 nm divided by the steady-state average cargo velocity*).

(5) <u>Sensitivities to model assumptions and parameters</u>

As stated in the main text, the rate that a multiple motor complex’s filament-bound configuration evolves in time will depend on inter-relationships between its mechanical and mechanochemical properties, all of which are nonlinear functions of the applied load. Below, we evaluate the sensitivities of two-kinesin transport behaviors to the treatments of these functions, particularly with respect to motor detachment kinetics. Overall, these analyses illustrate the importance of enumerating a full range of microstates in a model, and highlight the central need to accurately approximate the difference in strain energies associated with transitions between these microstates. Treatments of load-rate-dependent effects are also important, but with respect to composite behaviors, the combined effects of the strain-dependence to motor binding and the absence of load sharing due to kinesin’s efficient mechanochemistry (*mode A F-V dependence*) tends to dominate the average behaviors of the motors, producing generically-weak responses to motor copy number. Treatment of the loading rates (*the decreased load rate experienced by the motors at low applied loads*) is necessary to refine model predictions and, especially, to best reproduce the observed dependence of the microstate detachment transitions from two-motor-bound configurations to single-motor-bound configurations <$k_{\mathrm{off}[2\rightarrow 1]}$>.

5.1 Importance of considering the strain-dependence of motor binding rates

Analyses of detachment forces indicate the treatment of the strain dependence of motor binding as specified in equation S10 is very important to reproducing the generic shape of our measured detachment force distribution (Fig. S3A). Without this treatment, a second the peak in the detachment force distribution at 9.5 appears that is not in our data. Although detachment rates are essentially unaffected by this change, the overall force production is much more additive.

The above result suggests the mechanical work required to move an unbound motor in a two-motor system to a particular microtubule lattice site (*which is equal to the difference in configurational energy between the two geometries*) will, according to Arrhenius theory, reduce the rate of that transition exponentially. Strain (*elastic energy*) therefore reduces the total rate of binding into all microstates and generally dictates that the second motor would bind to lattice sites at which it does not experience load, meaning that in order to share load with the first motor it would have to narrow the separation distance between them through stepping. This effect likely contributes to the distinction of the mode A and mode B results described in the text, given that the difference in these stepping behaviors influences how rapidly motor can catch one another when bound to the microtubule.

5.2 Sensitivity of multiple motor dynamics to the motor detachment behaviors

We tested several permutations of our motor detachment treatment to assess whether exponential fits (Kramer's model) are sufficient to reproduce the two-motor detachment force and transition rate trends present in the trapping data. As discussed below, these analyses indicate a need to enhance the detachment rates of motors within a complex (*from two-motor-bound microstates*) over those of single motor molecules experiencing the same force to reproduce the single peak observed in the two-kinesin detachment force distribution. Therefore, the absence of load sharing cannot account for the shape of this distribution or the load dependence of $k_{\text{off}[2\rightarrow 1]}$ alone. This result indicates that appropriate treatments of load-rate-dependent effects are important in describing multiple-kinesin behaviors. Furthermore, best agreement between detachment force and $k_{\text{off}[2\rightarrow 1]}$ trends are observed when the full model treatment is implemented. These results are summarized below.

5.2.1 <u>*Deviations assuming a Kramer's-like single-exponential detachment behavior*</u>*.* Multiple exponential fits to the single kinesin data were generated (*e.g., over the full data range and while omitting the high-force data point*) to more fully test the appropriateness of this treatment of single-motor detachment data (Fig. S1A). As with the removal of the strain-dependence to motor binding, parameterizing motor detachment rates using any of these fits produces two peaks in the detachment force distribution (Fig. S2B). Furthermore, the two-motor detachment rate $k_{\text{off}[2\rightarrow 1]}$ is generally much lower than the data and nearly smooth, whereas the data is highly non-monotonic. These results clearly suggest that the average detachment rate of one or both of the motors in the two-motor system must be higher than those observed in our single motor assays.

5.2.2 <u>*Sensitivities to the treatment of load-rate-dependent effects*</u>*.* A treatment where the two-state model is used to parameterize motor detachment exclusively (*i.e., this assumes load rates experience by motors are not attenuated by collective effects*) produces qualitatively similar behaviors as the single-exponential fit (Fig. S3A), although the high force peak in the detachment force distributions is somewhat less pronounced. In addition, the non-monotonic character of $k_{\text{off}[2\rightarrow 1]}(F_{ap})$ is reproduced to a larger degree than with the Kramer's treatment (Fig. S3D). This occurs due to the higher curvature of the single-motor detachment fit near the stalling force of the motor. Nevertheless, despite this behavior, calculated $k_{\text{off}[2\rightarrow 1]}(F_{ap})$ rates greatly under-approximate measured detachment rates as low applied loads in the two motor case.

An analogous treatment where motor detachment is assumed to follow the load-rate-independent detachment trend produces a single peak in the detachment force distribution, but appears to over-approximate the $k_{\text{off}[2\rightarrow 1]}$ rates at high forces (Fig. S2B). Our complete model possesses a mixture of these behaviors, and best reproduces the high detachment rates (*low affinity and extensive negative motor cooperation*) below kinesin's stalling force, and the

increased affinities observed due to the predominance of load sharing above kinesin's stalling force.

5.2 Sensitivity of the model of motor stepping

The model of Fisher and Kim provides a relatively simple framework to define motor stepping efficiencies while allowing treatment of vectorial forces within in multiple-motor systems. In comparison, empirical fits to single-kinesin data cannot implicitly account for the direction of the load vector on the motor; stalk angles of motor within a complex can be different that those of single motor molecules experiencing the same loading force in the x-direction. Nevertheless, in the model of Fisher and Kim, motor stepping rates vary moderately with stalk angle (*the amount of work in the 'z' direction is usually small because the displacement is small*), so this treatment mostly refines the results rather than changing them qualitatively.

It is also important to note that the explicit treatment of back stepping is not necessarily critical to capturing multiple kinesin dynamics since this transition rate is small compared to kinesin's forward stepping rate until applied loads become very large. Thus, similar behaviors will emerge if the backward stepping rates are removed from the master equations describing the two-kinesin system. However, this will not be the case for other classes of motors whose velocities change with load via a larger modulation of their backward stepping rate. Multiple motor systems of such motors can be analyzed much more easily through modifications to the parameters in the Fisher-Kim model.

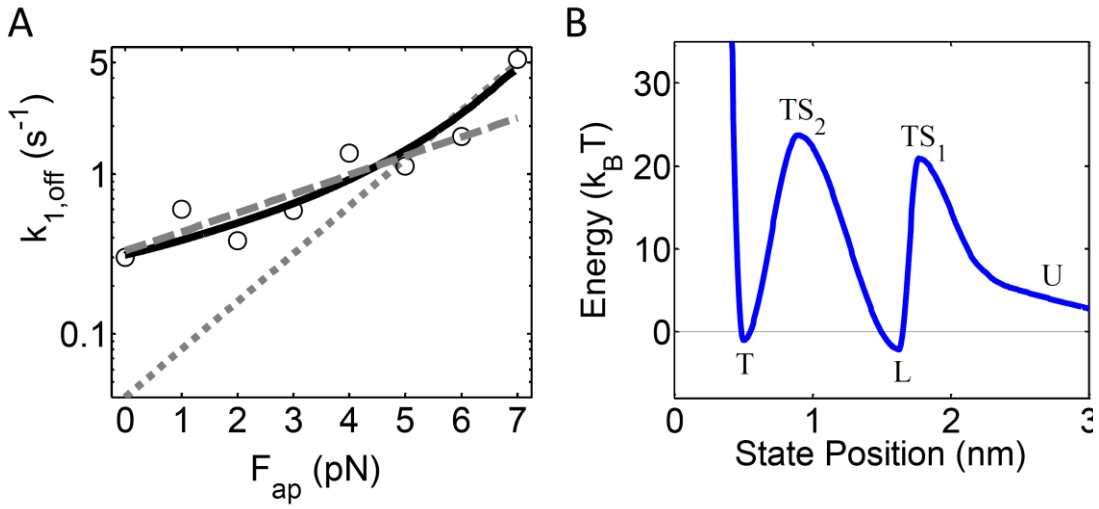

FIGURE S1. (**A**) Log plot of single kinesin detachment rates and fits. The single exponential fit to the full data set (*dotted line*) and to the first seven points (*dashed line*) show less agreement with the data than the load-rate-dependent model (*black line*) and tend to under-approximate motor detachment rates. (**B**) Motor-microtubule detachment reaction coordinate and its effects on the two-kinesin detachment force distribution. Energies and positions of the tightly bound (T), loosely bound (L), and unbound (U) states as well as those of the transition states in between are depicted in the plot above. All values are derived from the simulation and fitting procedure for the two-state model described in Section 3.1.

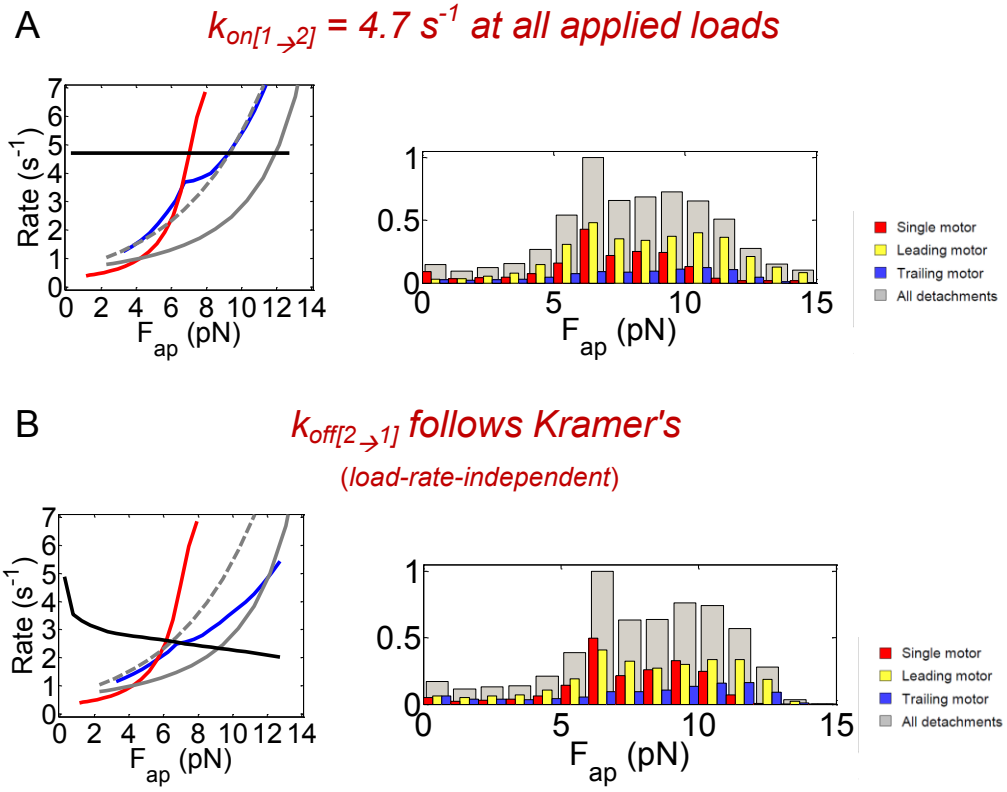

FIGURE S2. Effects of strain-dependent binding and load-rate-dependent model of detachment. Transition rates (*left*) and detachment force histograms (*right*) when (**A**) binding is strain-independent and (**B**) when a single-exponential model of detachment is used. In both cases, detachment force distributions show more additive function than the model presented in the main text. Two-motor detachment rates in **B** are much lower and show less non-monotonic character than in our complete model.

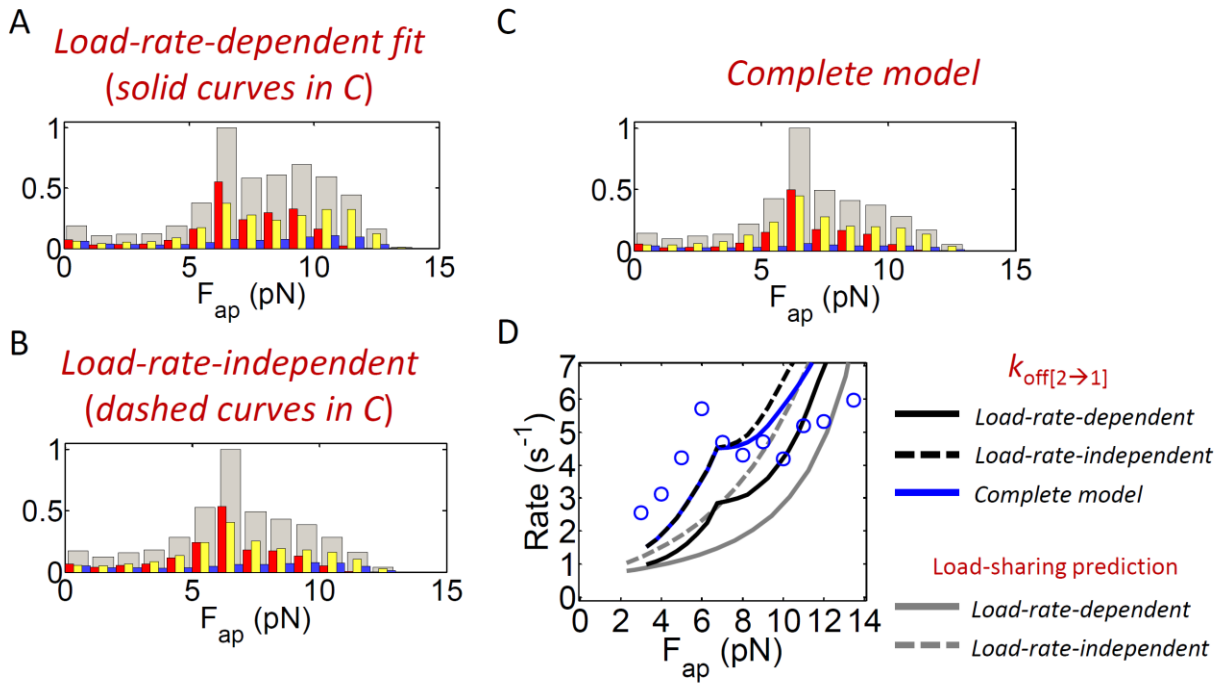

FIGURE S3 Two-kinesin detachment force distributions, produced assuming motor detachment follows (**A**) the two-state model's load-rate-dependent fit in Fig. 2C of the text, (**B**) the corresponding load-rate-independent prediction, and (**C**) the complete model. (**D**) Plots of the detachment rate $k_{\mathrm{off}[2\rightarrow 1]}(F_{ap})$ for each model treatment.

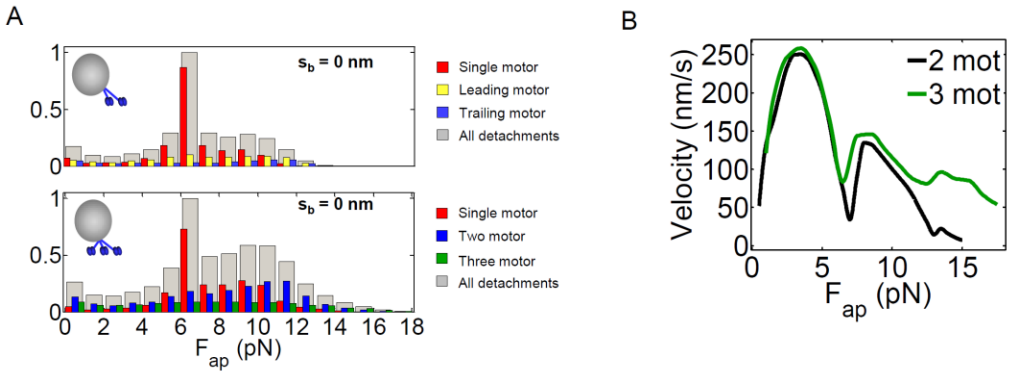

FIGURE S4. Effects of separation distance at the bead and a third kinesin. (**A**) Detachment force distributions with a breakdown of events for kinesins anchored to the same point on the bead surface. Kinesins follow the same switching detachment dependence employed to approximate the data in the main text (Fig. 3A). The two-kinesin distribution (*top*) shows that the system is slightly less cooperative than the one with a 50 nm separation distance at the bead. The three-kinesin distribution (*bottom*) shows that adding a third kinesin enhances the activity of the complex, but only enough to give two peaks, the tallest still being near kinesin's stall force. The breakdown consists of all detachment events beginning in three-motor-bound microstates (*green*), two-motor-bound microstates (*blue*), and single-motor-bound microstates (*red*). (**B**) Bead velocities as a function of applied load for the systems analyzed in **A** show that cargos are driven by *n* load-sharing kinesins when they experience loads less than ~n*F_s, where F_s is the stall force of a single kinesin.

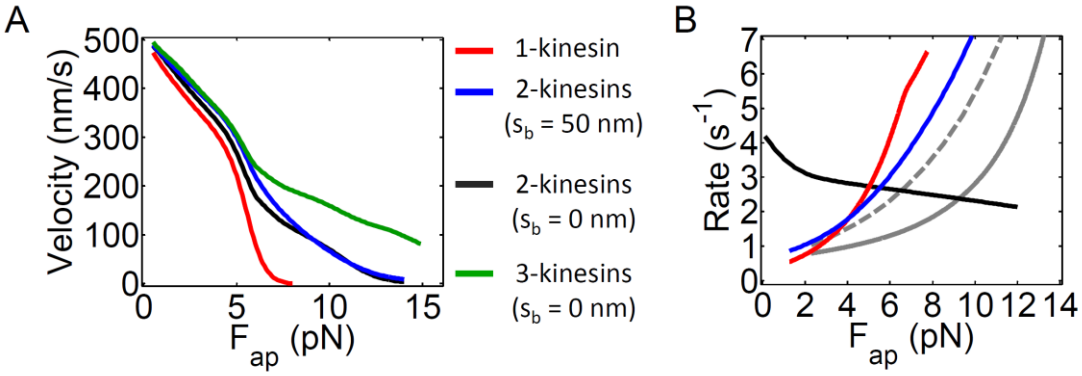

FIGURE S5. Kinesin-driven bead velocities and transition rates under constant applied loads. (**A**) Average bead velocities as a function of applied load for a single kinesin (*red*), two kinesins (s_b = 50 nm, *blue*; s_b = 0 nm, *black*), and three kinesins (*green*) demonstrate that load sharing does not occur below the stall force of a single kinesin even when loads are held constant and the motors are given time to reach their steady-state separation distance(s). (**B**) Motor binding rates (*black*) are very similar to those measured in the static trap (Fig. 3D). The detachment rate $\langle k_{off[2\rightarrow 1]}(F_T)\rangle$ (*blue*) shows a monotonic increase with load, in contrast to the dependence found in the static trap. Equal-load-sharing predictions for motors with steady-state detachment dependence (*dashed grey*) and non-steady-state, single-motor fitted detachment dependence (*solid grey*) are presented for comparison. The single-motor detachment rate $\langle k_{off[1\rightarrow 0]}(F_T)\rangle$ (*red*) comes from the load-rate independent behavior in Fig. 2C of the main text.

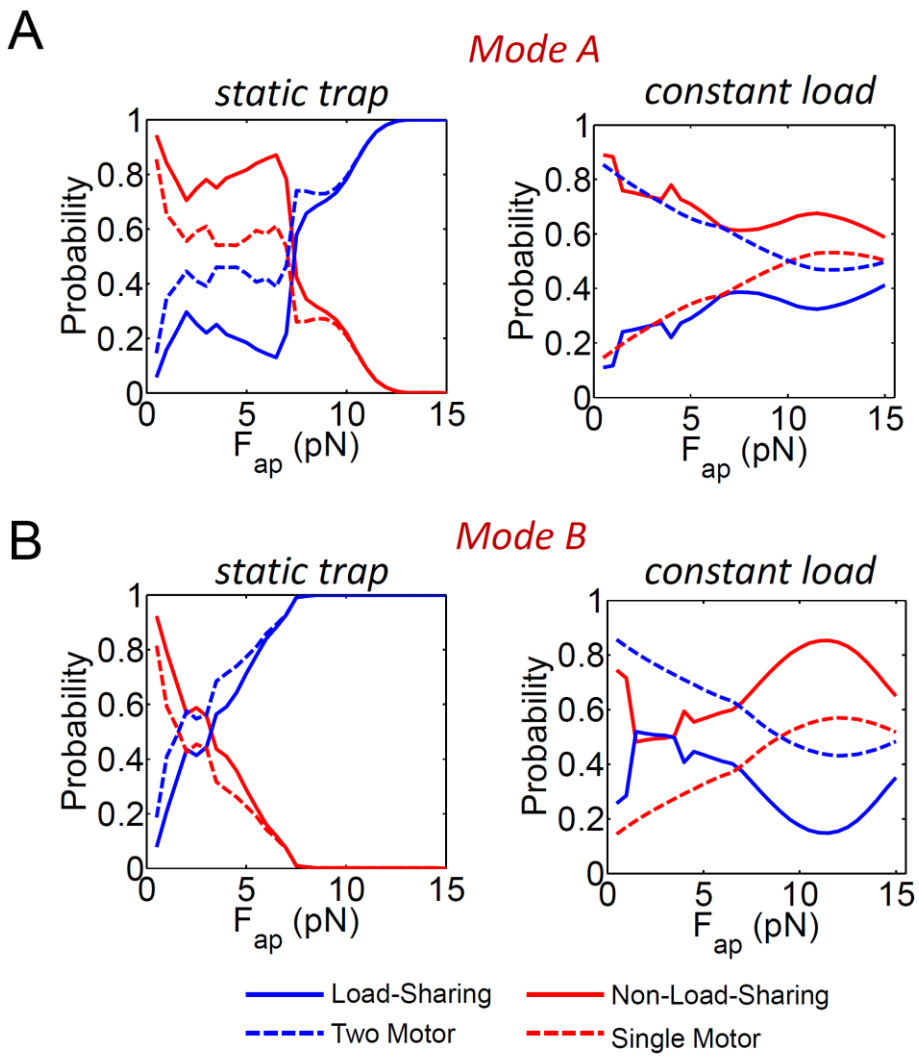

FIGURE S6. Probability of two-motor-bound and load sharing fractions as a function of applied load. In each plot, single and two-motor-bound microstate populations are plotted (*dashed lines*), as well as the load-sharing and non-load-sharing microstate populations (where "load sharing" means that both motors carry at least 35% of the total load, *solid lines*). Red is used to denote single-motor or non-load-sharing populations while blue is used for two-motor or load-sharing populations. (**A** and **B**) Results for stepping modes A and B, respectively, are shown for both increasing (*left*) and constant loads (*right*).

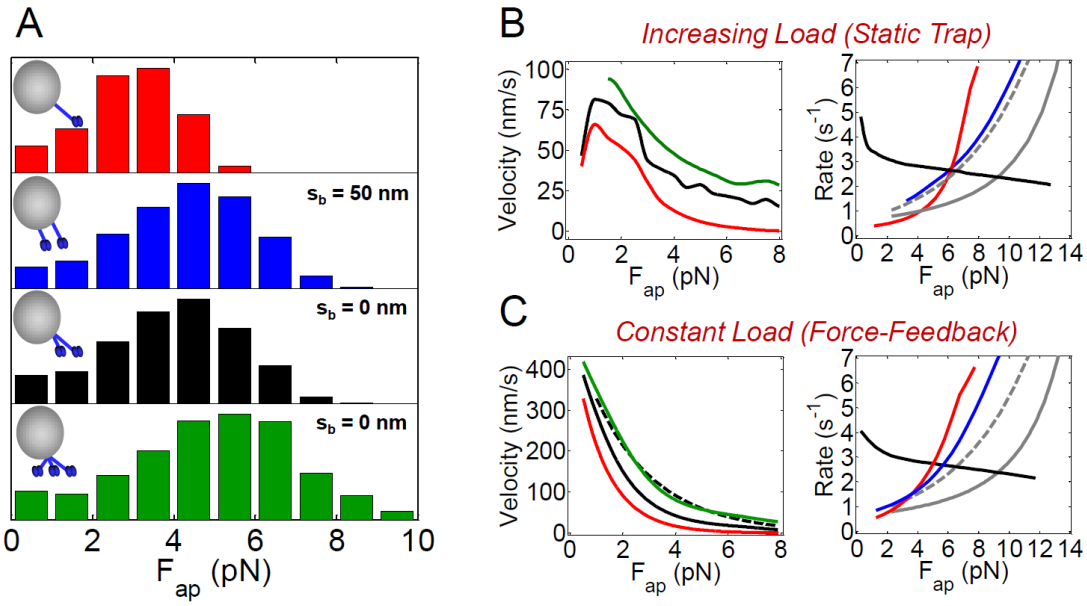

FIGURE S7. Multiple-motor transport against increasing and constant loads (stepping mode B). (**A**) Calculated detachment force distribution histograms for a single motor and multiple motor complexes in a static optical trap. The total motor number and on-bead motor separation distance (s_b) is shown in each panel. (**B** and **C**) Average motor binding / detachment transition rates and *F-V* curves calculated assuming cargos are transported against increasing (**B**) or constant (**C**) applied loads. Transition rates describing motor binding ($k_{on[1\rightarrow 2]}$, *black line*) and detachment ($k_{off[1\rightarrow 0]}$, *red line*, and $k_{off[2\rightarrow 1]}$, *blue line*). The grey lines in the transition rate plots correspond to the expected detachment rates under equal load sharing for the load-rate-dependent fit (*solid*) and the load-rate-independent calculation (*dashed*). Line colors in the *F-V* plots correspond to those used to designate motor number and s_b in **A**.

Supporting References

1 Leduc, C., O. Campás, K.B. Zeldovich, A. Roux, P. Jolimaitre, L. Bourel-Bonnet, B. Goud, J.-F. Joanny, P. Bassereau, and J. Prost. 2004. Cooperative extraction of membrane nanotubes by molecular motors. *Proc. Natl. Acad. Sci. USA*. 101:17096-17101.

2 Jamison, D.K., J.W. Driver, A.R. Rogers, P.E. Constantinou, and M.R. Diehl. 2010. Two kinesins transport cargo primarily via the action of one motor: implications for intracellular transport. *Biophys. J.* 99:2967-2977.

3 Jeney, S., E.H.K Stelzer, H. Grubmüller, and E.-L. Florin. 2004. Mechanical properties of single motor molecules studied by three-dimensional thermal force probing in optical tweezers. *ChemPhysChem* 5:1150-1158.

4 Evans, E. 2001. Probing the relation between force-lifetime-and chemistry in single molecular bonds. *An. Rev. Biophys. Biomol. Struct.* 30**:**105-128.